A mathematical model coupling polarity signaling to cell adhesion explains diverse cell migration patterns

William R. Holmes[1]*, JinSeok Park[2], Andre Levchenko[2], Leah Edelstein-Keshet[3]

1 Department of Physics and Astronomy, Vanderbilt University, Nashville, Tennessee, United States of America, **2** Department of Biomedical Engineering, Yale University, New Haven, Connecticut, United States of America, **3** Department of Mathematics, University of British Columbia, Vancouver BC, Canada

* william.holmes@vanderbilt.edu

Abstract

Protrusion and retraction of lamellipodia are common features of eukaryotic cell motility. As a cell migrates through its extracellular matrix (ECM), lamellipod growth increases cell-ECM contact area and enhances engagement of integrin receptors, locally amplifying ECM input to internal signaling cascades. In contrast, contraction of lamellipodia results in reduced integrin engagement that dampens the level of ECM-induced signaling. These changes in cell shape are both influenced by, and feed back onto ECM signaling. Motivated by experimental observations on melanoma cells lines (1205Lu and SBcl2) migrating on fibronectin (FN) coated topographic substrates (anisotropic post-density arrays), we probe this interplay between intracellular and ECM signaling. Experimentally, cells exhibited one of three lamellipodial dynamics: persistently polarized, random, or oscillatory, with competing lamellipodia oscillating out of phase (Park et al., 2017). Pharmacological treatments, changes in FN density, and substrate topography all affected the fraction of cells exhibiting these behaviours. We use these observations as constraints to test a sequence of hypotheses for how intracellular (GTPase) and ECM signaling jointly regulate lamellipodial dynamics. The models encoding these hypotheses are predicated on mutually antagonistic Rac-Rho signaling, Rac-mediated protrusion (via activation of Arp2/3 actin nucleation) and Rho-mediated contraction (via ROCK phosphorylation of myosin light chain), which are coupled to ECM signaling that is modulated by protrusion/contraction. By testing each model against experimental observations, we identify how the signaling layers interact to generate the diverse range of cell behaviors, and how various molecular perturbations and changes in ECM signaling modulate the fraction of cells exhibiting each. We identify several factors that play distinct but critical roles in generating the observed dynamic: (1) competition between lamellipodia for shared pools of Rac and Rho, (2) activation of RhoA by ECM signaling, and (3) feedback from lamellipodial growth or contraction to cell-ECM contact area and therefore to the ECM signaling level.

Author summary

Cells crawling through tissues migrate inside a complex fibrous environment called the extracellular matrix (ECM), which provides signals regulating motility. Here we investigate one such well-known pathway, involving mutually antagonistic signalling molecules (small GTPases Rac and Rho) that control the protrusion and contraction of the cell edges (lamellipodia). Invasive melanoma cells were observed migrating on surfaces with topography (array of posts), coated with adhesive molecules (fibronectin, FN) by Park et al., 2017. Several distinct qualitative behaviors they observed included persistent polarity, oscillation between the cell front and back, and random dynamics. To gain insight into the link between intracellular and ECM signaling, we compared experimental observations to a sequence of mathematical models encoding distinct hypotheses. The successful model required several critical factors. (1) Competition of lamellipodia for limited pools of GTPases. (2) Protrusion / contraction of lamellipodia influence ECM signaling. (3) ECM-mediated activation of Rho. A model combining these elements explains all three cellular behaviors and correctly predicts the results of experimental perturbations. This study yields new insight into how the dynamic interactions between intracellular signaling and the cell's environment influence cell behavior.

Introduction

Migrating cells display polarization of many membrane and cytosolic components, and spatially inhomogeneous signaling activity. Cellular polarity can be highly dynamic, displaying random, persistent or even oscillatory patterns [1–3] with clear deterministic features [4, 5]. In spite of recently proposed phenomenological models attempting to explain how these polarity patterns can emerge in the absence of graded extracellular cues [5, 6], we still lack the mechanistic understanding of the dynamic molecular mechanisms underlying the polarity establishment and maintenance over the course of cell migration. Thus, given the complexity of the polarity dynamics, we still do not know if diverse spatio-temporal patterns can be accounted for by the same mechanistic framework, quantitatively embedded in a biochemically informed mathematical model. Having such a framework may assist in interventions aimed at enhancement or inhibition of persistence of cell migration in diverse setting, such as wound healing or aggressive cancer spread.

Aggressive cancers, such as advanced stage melanoma and glioblastoma multiforme, frequently display persistent cell migration away from the primary tumor site. In the context of melanoma, the invasive tumor spread is associated with several mutations, including the loss of functional expression of PTEN, and the corresponding increase in the activity of the PI3K-AKT signaling pathway. It is not clear how such mutations, affecting the state of the signaling and regulatory networks controlling multiple cellular functions, could influence cellular polarity dynamics and the persistence of cell migration. Migrating cells also frequently relocate to micro-environments that are distinct from those of the tissue of origin. One of the key aspects of cellular micro-environment is the organization and composition of the extracellular matrix. Alteration in the density, orientation and nano-topography of the extracellular matrix fibers and their cleaved fragments have been shown to be instrumental in onset of cellular spread and in defining the direction and persistence of cellular migration [7–9]. Recent analysis suggested that these matrix re-arrangements can be well approximated in experiments, using matrix-mimicking nano-fabricated platforms that allow for controlled variation of the model matrix structure and chemical composition [10]. In particular, in our experimental

analysis with melanoma cell lines we found that individual cells can display diverse polarity patterns when migrating in areas of the model matrix with various degrees of anisotropy [11]. Having this type of controlled micro-environment can allow one to develop mechanistic models [12] of cell polarity control and to test them by checking for consistency between model predictions and experimental results.

In this study, we focused on testing a set of alternative models against the experimental data obtained for melanoma cell lines of different degrees of invasiveness [13, 14]. Advanced stages of melanoma are characterized by one of the most invasive behaviors of any cancer, leading to rapid metastatic spread and dismal survival prognosis. In this stage, transformed melanocytes transition from radial to vertical spread patterns, invading the underlying collagen-rich dermis layer and penetrating the blood vessels. Cell polarity and ensuing cell migration patterns can define the effectiveness of the cell invasion, i.e, initial metastatic steps. The experimental dataset used in our analysis represented classification of cell polarization patterns into random, oscillatory and persistent, in the presence of diverse extracellular cues and pharmacological perturbations targeting specific molecular species implicated in polarization control.

Rho GTPases and extracellular matrix signaling

Rho GTPases are central regulators that control cell polarization and migration [15, 16], embedded in complex signaling networks of interacting components [17]. Two members of this family of proteins, Rac1 and RhoA, have been identified as key players, forming a central hub that orchestrates the polarity and motility response of cells to their environment [18, 19]. Rac1 (henceforth "Rac") works in synergy with PI3K to promote lamellipodial protrusion in a cell [16], whereas RhoA (henceforth "Rho") activates Rho Kinase (ROCK), which activates myosin contraction [20]. Mutual antagonism between Rac and Rho has been observed in many cell types [19, 21, 22], and accounts for the ability of cells to undergo overall spreading, contraction, or polarization (with Rac and Rho segregated to front versus rear of a cell).

The extracellular matrix (ECM) is a jungle of fibrous and adhesive material that provides a scaffold in which cells migrate, mediating adhesion and traction forces. ECM also interacts with cell-surface integrin receptors, to trigger intracellular signaling cascades. Important branches of these pathways are transduced into activating or inhibiting signals to Rho GTPases. On one hand, ECM imparts signals to regulate cell shape and cell motility. On the other hand, the deformation of a cell affects its contact area with ECM, and hence the signals it receives. The concerted effect of this chemical symphony leads to complex cell behavior that can be difficult to untangle using intuition or verbal arguments alone. This motivates our study, in which mathematical modeling of GTPases and ECM signaling, combined with experimental observations is used to gain a better understanding of cell behavior, in the context of experimental data on melanoma cells.

There remains the question of how to understand the interplay between genes (cell type), environment (ECM) and signaling (Rac, Rho, and effectors). We and others [19, 21–27] have previously argued that some aspects of cell behavior (e.g., spreading, contraction, and polarization or amoeboid versus mesenchymal phenotype) can be understood from the standpoint of Rac-Rho mutual antagonism, with fine-tuning by other signaling layers [28]. Here we extend this idea to couple Rac-Rho to ECM signaling, in deciphering the behavior of melanoma cells in vitro. There are several overarching questions that this study aims to address.

1. How does signaling and cell motility interface with external inputs to the cell? How does the change in cell shape (in protrusion/contraction) affect inputs to the signaling network and thus cell behavior?

2. Are diverse types of cell migration (random persistent, oscillatory) part of the same overall repertoire, or are they distinct and discrete?

3. How do constraints such as limited GTPase availability [27, 29–32], lamellipod competition [33, 34] and feedbacks (mutual inhibition, positive feedback) determine the cell behavior [35].

4. Can we understand the transition to invasive cancer cells as a shift in basic parameters of the same underlying signaling system?

Experimental observations constraining the models

In experiments of Park et al. [11] melanoma cells were cultured on micro-fabricated surfaces comprised of post density arrays coated with fibronectin (FN), representing an artificial extra-cellular matrix. The anisotropic rows of posts provide inhomogeneous topographic cues along which cells orient.

In [11], cell behavior was classified using the well-established fact that PI3K activity is locally amplified at the lamellipodial protrusions of migrating cells [36]. PI3K "hot spots" were seen to follow three distinct patterns about the cell perimeters: random (RD), oscillatory (OS), and persistent (PS). These classifications were then associated with three distinct cell pheno-types: persistently polarized (along the post-density axis), oscillatory with two lamellipodia at opposite cell ends oscillating out of phase (protrusion in one lamellipod coincides with retrac-tion of the other, again oriented along the post-density axis), and random dynamics, whereby cells continually extend and retract protrusions in random directions. The fraction of cells in each category was found to depend on experimental conditions.

Here, we focus on investigating how experimental manipulations influence the fraction of cells in different phenotypes. For simplicity, we focus on the polarized and oscillatory pheno-types which can be most clearly characterized mathematically. The following experimental observations are used to test and compare our distinct models of cell signaling dynamics.

(O1). Rho is known to activate Rho Kinase (ROCK), which phosphorylates myosin light chain and leads to actomyosin contraction. Inhibiting ROCK is observed to increase the fraction of polarized and decrease the fraction of oscillatory cells.

(O2). More invasive melanoma cell lines (1205Lu) are enriched in PI3K and low in the antag-onist PTEN. These cells exhibit a lower fraction of random cells and higher fractions of persistently polarized and oscillatory cells than the less invasive melanoma cell line SBcl2.

(O3). Increasing fibronectin level on the post density array surfaces increases the fraction of oscillatory and lowers the fraction of persistently polarized cells.

For a graphical summary of cell phenotypes and experimental observations, see Fig 1.

Results

We use experimental observations (O1–3) as indirect constraints, to distinguish hypotheses for how feedbacks between internal cellular signaling and external ECM inputs modulate cel-lular behaviors. Toward this end, we construct a collection of simple, predictive models for Rac-Rho-ECM signaling, and compare model predictions to observations (O1–3) to determine which hypotheses are most consistent with experimental results. The activities of the small GTPases Rac and Rho are used as surrogates for the Rac1/PI3K and RhoA/ROCK pathways that respectively promote actin-based protrusion and acto-myosin based contraction in
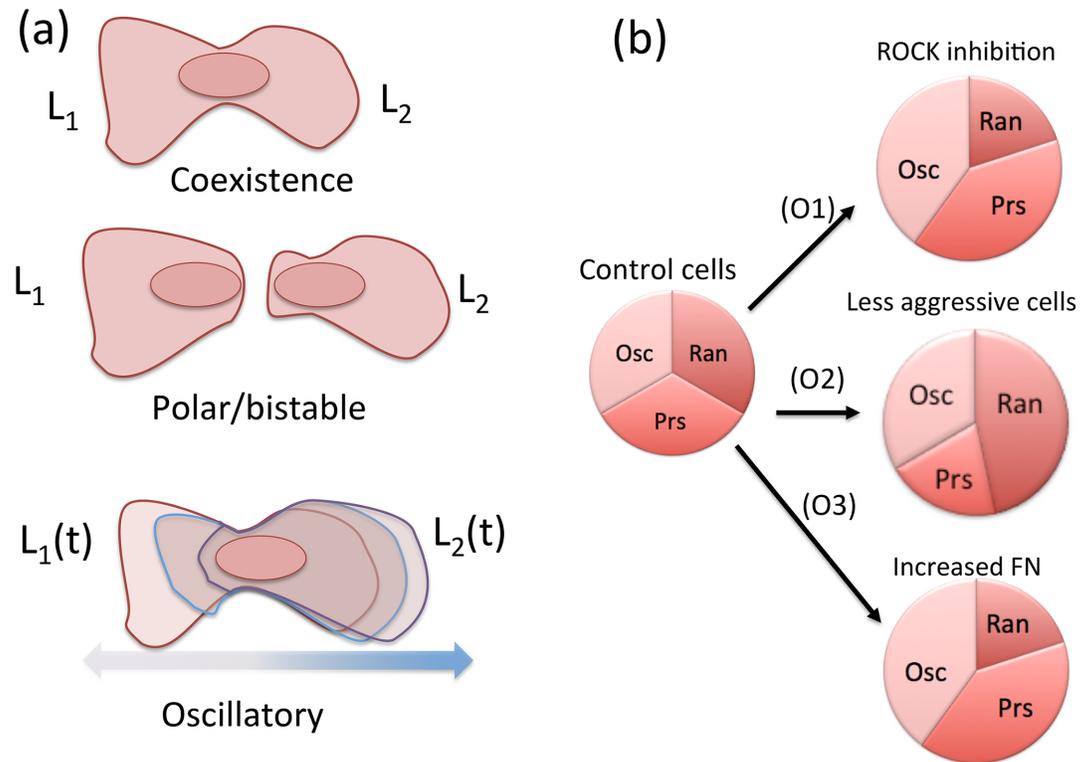
Fig 1. Cell phenotypes and experimental observations. In modeling melanoma cells, we consider signaling and competition of two lamellipodia (indicated by L_1, L_2). **(a)** Cell states described by our models include (top to bottom) coexistence of two lamellipodia, polarization in which one lamellipod "wins" the competition (also includes bistability where initial conditions determine the eventual polarity direction), and antiphase oscillations in which one lamellipod expands while the other contracts periodically. The ECM variables E_1, E_2 are surrogates for both lamellipod size and ECM signaling activity. **(b)** (Approximate) experimental observations agains which proposed models are tested. Relative to control cells, those with either ROCK inhibition or exposed to high fibronectin (FN) level have a lower fraction of randomly directed (apolar) cells, whereas the less aggressive cells have a lower fraction of persistently polarized cells.

lamellipodia. Based on prior observations [18, 19, 22, 26, 27, 37, 38], we assume that Rac and Rho are mutually inhibitory. We also assume that sufficiently high levels of ECM signaling upregulates the activity of RhoA [39, 40]. There is evidence that ECM signaling can also upregulate Rac to some extent, e.g. [41, 42]. In the final model (Model 3) discussed here, we consider the possibility that ECM influences Rac activation as well. However based on our analysis, for reasons that will become clear in the Discussion, we assume that Rho activation is the dominant effect of ECM signaling. While motility regulation is vast with numerous regulators and interactions, we ask what aspects of cell behavior can be explained by this core signaling unit, and take the view that other parts of the signaling cascade serve to fine tune model parameters and inputs.

To compare models to data, we consider three cell states: apolar, persistently polarized, and oscillatory (Fig 1). We interpret these, respectively, in terms of the competition of two lamellipods that can either coexist, exclude one another, or cycle through antiphase oscillations where each grows at the expense of the other [11]. Apolar cells are identified with the "random" state described in [11], lacking directionality and subject to stochastic fluctuations of polarity (not explicitly modelled). Each lamellipod is represented as a spatially well-mixed compartment. Hence, our models consist of ordinary differential equations describing the
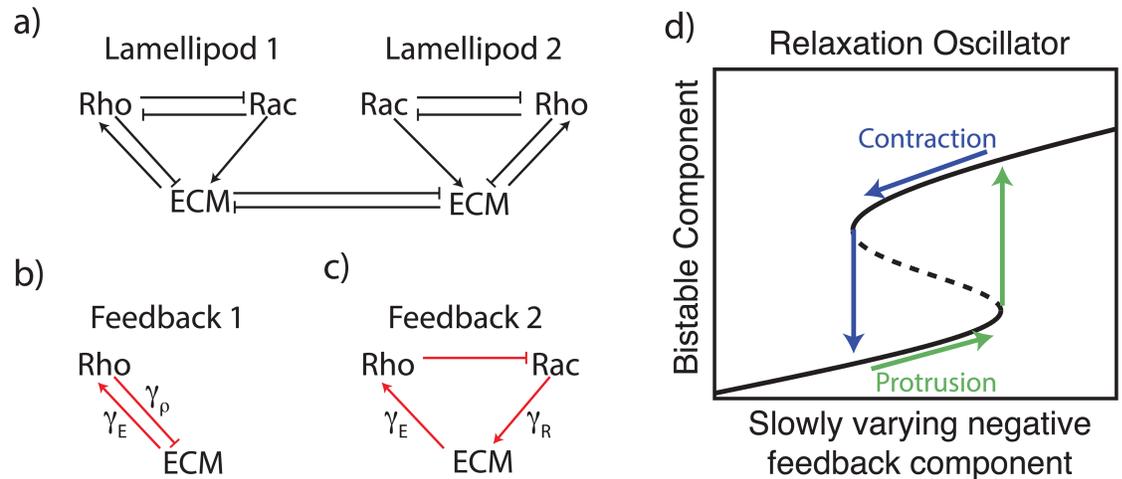
Fig 2. Model schematic. (a) Schematic depiction of the proposed interactions between the GTPases and cell-ECM contact areas, which are proxies for extracellular matrix (ECM) signalling in each lamellipod (E_j). We assume that Rac (Rho) promotes protrusion (contraction), resulting in opposite effects: Rac (Rho) increases (decreases) the cell-ECM contact area and hence E_j. Mechanical constraints or other limitations couple the two lamellipods, preventing the cell-ECM contact areas from growing independently. This is modelled as a competition term coupling E_1 and E_2. **(b,c)** We consider two potential negative feedback loops that could lead to oscillations. Each arrow is labeled with the parameter governing the strength of its influence. **(d)** Basic idea of a relaxation oscillator: bistability is present in a subset of the model (black curve); other component(s) acting on a slower timescale provide negative feedback that sets up oscillations (green, blue curves). In this illustration, bistability results from two fold bifurcations as in the GTPase submodel, but the same idea applies when the bifurcations are both transcritical, as found in the ECM submodel (Fig 3d). Protrusion causes an increase in ECM signaling that leads to increased feedback, contraction has the opposing effect.

dynamics and interactions of Rac and Rho within and between these compartments. More-over, we adopt a caricature of cell-substratum contact area as ECM signaling level, which means that lamellipod size is synonymous with our ECM activity variable. Hence, high Rac activity is assumed to promote ECM signaling (via lamellipod protrusion), whereas high Rho activity has an ECM inhibiting effect (due to lamellipod contraction).

A schematic diagram of the signaling model we discuss is shown in Fig 2(a). This overarch-ing model depicts mutually antagonism of Rac and Rho [18, 19, 21, 23, 24, 27, 28], and compe-tition of the two lamellipods, assuming growth of one suppresses that of the other. (In the model, lamellipod size is synonymous with cell-ECM contact area and with the level of ECM signaling.) We also assume that the influence of ECM signaling is primarily on Rho activity. Our models differ by details of the feedbacks and other key assumptions. Fig 2(b) and 2(c) fur-ther illustrate the feedbacks between internal GTPase signaling and ECM signaling layers.

It is well known that mutual inhibition (or mutual competition) can set up bistability and hysteresis. Furthermore, bistability coupled to slow negative feedback can lead to oscillations [43]. This idea forms the central theme in our models (Fig 2d). Moreover, as we will argue, this idea can account for all three observed phenotypes (in appropriate parameter regimes), namely a single "winning" lamellipod (persistent polarization), apolarity (coexisting lamellipods) and cycling (antiphase oscillations of growth and decay of the two lamellipods). The question we address, then, is which subsystem sets up bistability and which leads to oscillations; various interactions between GTPase and ECM signaling levels could, in principle, account for each. One goal of our modeling is to tease apart the possibilities and find the most likely signaling model that best accounts for experimental observations (Section "Experimental observations constraining the models").

Table 1. We describe the qualitative elements of each model that give rise to polarity and antiphase lamellipod oscillations, respectively. MM: Michaelis Menten kinetics. Numbers indicate the model designation used in the text.

	Source of Polarity	Source of anti-phase oscillations
Lamellipod Competition (1)	Bistable lamellipod coupling	Fast ECM / Slow GTPase feedback
	Conserved GTPase with MM kinetics	Bistable lamellipod coupling
Bistable GTPase (2)	Bistable GTPase model	Slow ECM / Fast GTPase feedback
	Monostable lamellipod coupling	Monostable lamellipod coupling
Hybrid (3)	Conservative GTPase model with Hill kinetics	Slow ECM / Fast GTPase feedback
	Monostable lamellipod coupling	Monostable lamellipod coupling

https://doi.org/10.1371/journal.pcbi.1005524.t001

As in most models of intracellular signalling, obtaining biologically accurate values of rate parameters from direct biochemical measurement is unrealistic. Hence, we use the following strategy to parametrize our models. First, we scale the state variables in terms of their inherent "IC$_{50}$" levels (levels at which Hill functions are at 50% of their maximal magnitude). We also scale time by GTPase inactivation times. This scaling yields a smaller number of ratios of parameters to estimate, i.e. ratios that represent scaled basal and feedback-induced activation rates. For simplicity, we assume that parameters of the Rac and Rho equations are relatively similar.

Modeling overview

We discuss three model variants, each composed of (A) a subsystem endowed with bistability, and (B) a subsystem responsible for negative feedback. In short, Model 1 assumes ECM competition for (A) and feedbacks mediated by GTPases for (B). In contrast, in Model 2 we assume GTPase dynamics for (A) and ECM mediated feedbacks for (B). Model 3 resembles Model 2, but further assumes limited total pool of each GTPase (conservation), which turns out to be a critical feature. See Tables 1 and 2 for details.

We analyze each model variant as follows: first, we determine (bi/mono)stable regimes of subsystem (A) in isolation, using standard bifurcation methods. Next, we parameterize subsystem (B) so that its slow negative feedback generates oscillations when (A) and (B) are coupled in the model as a whole. For this to work, (B) has to force (A) to transition from one mono-stable steady state to the other (across the bistable regime) as shown in the relaxation loop of Fig 2d. This requirement informs the magnitude of feedback components. Although these considerations do not fully constrain parameter choices, we found it relatively easy to then parameterize the models (particularly Models 1b and 3). This implies model robustness, and suggests that broad regions of parameter space lead to behavior that is consistent with experimental observations.

Rac-Rho signaling. Our underlying Rac-Rho model follows closely on the well-mixed version described in [27]. For each GTPase in each lamellipod, we assume a basic activation-

Table 2. Terms that represent the GTPase and lamellipod coupling in each sub-model.

	GTPase Model	Lamellipod coupling
Lamellipod Competition (1)	Michaelis Menten + conservation	Bistable, Species competition type equations
Bistable GTPase (2)	Bistable Hill kinetics	Monostable
Hybrid (3)	Hill kinetics + conservation	Monostable

https://doi.org/10.1371/journal.pcbi.1005524.t002

inactivation differential equation of the form

$$\frac{dG_k}{dt} = A_G G_I - \delta_G G_k, \qquad G = R, \rho. \tag{1a}$$

Here $G = R, \rho$ represent concentrations of active Rac and Rho, respectively, $G_I = R_I, \rho_I$ represent inactive GTPase levels, and $k = 1, 2$ (e.g. R_k) indicates the level in the k'th lamellipod. We assume the inactive GTPase pool is shared by competing lamellipods, but later incorporate different hypotheses about the size of this pool and the extent to which it is depleted. In some model variants, we assume that GTPases are abundant so that R_I, ρ_I are constant, whereas in other variants, the total GTPase is limited and conserved

$$R_I = R_T - R_1 - R_2, \quad \rho_I = \rho_T - \rho_1 - \rho_2, \tag{1b}$$

where R_T and ρ_T are total average concentrations of the GTPases (see Table 3).

We generally assume that mutual antagonism between Rac and Rho influences the rates of activation $A_{R,\rho}$, whereas the rate of inactivation, $\delta_{R,\rho}$, is constant. (This choice is largely arbitrary and implies GEF-based crosstalk [30, 44].) Typical terms are decreasing Hill functions, as shown in Table 3 and Eq (3). If $n = 1$ (i.e. Michaelis Menten kinetics) the Rac-Rho system will be monostable, whereas for $n > 1$ and appropriate parameters, the Rac-Rho system is bistable.

Extracellular matrix input. The extracellular matrix (ECM) provides input to GTPase signaling. However, the contact area between the cell and the ECM modulates that signaling since larger or smaller lamellipodia receive different levels of stimuli from the ECM. We define the variable E_k to represent both the cell-ECM contact area of the k'th lamellipod (for $k = 1, 2$) and the "effective level of ECM signaling" in the k'th lamellipod. (The larger the contact area, the more integrin receptors are engaged, the greater the stimuli received from the ECM by the given lamellipod.) Then Rac-driven cell protrusion and Rho-driven cell contraction will affect E_k on some timescale $1/\hat{\epsilon}$. We also consider the effect of competition between lamellipods for growth so that their "areas" (E_j, E_k) cannot expand independently. Mechanical tension or other limited shared resources mean that one lamellipod could only grow at the expense of the other. For example, Tony Y.-C. Tsai and Julie Theriot observe that neutrophil-like HL-60 cells confined to "quasi-2D" motion under an agarose pad have a constant total projected area, for which protruding and contracting lamellipodia compete (personal communication). Such

Table 3. Terms and notation used in model equations. Model 1: GTPase bistability, Model 2: Lamellipod competition, Model 3: Hybrid model. Parameters $\bar{\gamma}_{E,R,\rho}$ have similar meanings as $\gamma_{E,R,\rho}$ in Models 1,3 but carry distinct units to accommodate linear versus Hill function kinetic terms.

Parameter definition	Notation	Model 1	Model 2	Model 3
Rac activation rate	$A_R(\rho)$	$\dfrac{\hat{b}_R}{(\hat{\rho}_0 + \rho)}$	$\dfrac{\hat{b}_R}{(\hat{\rho}_0^3 + \rho^3)}$	$\dfrac{\hat{b}_R}{(\hat{\rho}_0^3 + \rho^3)}$
Rho activation rate	$A_\rho(R)$	$\dfrac{\hat{b}_\rho}{(\hat{R}_0 + R)}$	$\dfrac{\hat{b}_\rho}{(\hat{R}_0^3 + R^3)}$	$\dfrac{\hat{b}_\rho}{(\hat{R}_0^3 + R^3)}$
ECM effect on Rho activation	$b_\rho(E_k)$	$k_E + \bar{\gamma}_E E_k$	$k_E + \gamma_E \dfrac{E_k^3}{E_0^3 + E_k^3}$	$k_E + \gamma_E \dfrac{E_k^3}{E_0^3 + E_k^3}$
Protrusion; ECM growth rate	$P(R_k, E_k)$			
- - Basal Rac-dependent term	$B_E(R_k)$	0	$k_R + \gamma_R \dfrac{R_k^3}{R_0^3 + R_k^3}$	$k_R + \gamma_R \dfrac{R_k^3}{R_0^3 + R_k^3}$
- - ECM autoamplif. term	$A_E(R_k)$	$k_R + \bar{\gamma}_R R_k$	0	0
Rho dependent contraction	$L_E(\rho_k)$	$k_\rho + \bar{\gamma}_\rho \rho_k$	$k_\rho + \gamma_\rho \dfrac{\rho_k^3}{\rho_0^3 + \rho_k^3}$	$k_\rho + \gamma_\rho \dfrac{\rho_k^3}{\rho_0^3 + \rho_k^3}$
Total GTPase conserved	G_T	(2a) no; (2b) ✓	no	✓

observations could be modelled in many different ways. Here we chose the simplest appropriate "species competition" term to capture the main idea. This suggests that a reasonable model would be

$$
\begin{aligned}
\frac{dE_k}{dt} &= \hat{\epsilon}\left[\text{Protrusion} - \text{Contraction} - \text{Competition}\right] \\
&= \hat{\epsilon}\left[P(R_k, E_k) - C(\rho_k, E_k) - l_c E_k E_j\right],
\end{aligned}
\tag{2a}
$$

where l_c describes the strength of direct lamellipodia competition ($l_c = 0$ indicates no competition). We consider a combination of basal and self-enhanced components of the protrusion term P, as shown in Table 3. The Rho-dependent contraction term also captures competition of the lamellipods for growth. We will refer to E_k interchangeably as "ECM signaling level" and "lamellipod size" in our models, with the understanding that these two cell features are intimately linked.

Dimensionless model equations: General case. We nondimensionalize time by δ_ρ and GTPase levels by associated Hill function "IC$_{50}$ parameters" $\hat{R}_0, \hat{\rho}_0$ (See S1 Text) to arrive at a generic model formulation for the signaling dynamics in each lamellipod k ($k = 1, 2$):

$$
\frac{dR_k}{dt} = A_R R_I - \delta R_k, \qquad A_R = \frac{b_R}{1 + \rho_k^n},
\tag{3a}
$$

$$
\frac{d\rho_k}{dt} = A_\rho \rho_I - \rho_k, \qquad A_\rho = \frac{b_\rho(E_k)}{1 + R_k^n},
\tag{3b}
$$

$$
\frac{dE_k}{dt} = \epsilon\left[(B_E + A_E E_k) - E_k\left(L_E E_k + l_c E_j\right)\right], \quad j \neq k.
\tag{3c}
$$

Here, ϵ, δ are ratios of timescales and b_R, b_ρ are dimensionless. B_E, A_E, and L_E represent basal protrusion, auto-amplified protrusion, and contraction strength terms, which can depend on Rac and Rho concentrations. Rather than nondimensionalizing E_k, we retain l_c, the only parameter with units of E. This allows us to easily control the strength of coupling between the two lamellipods in our simulations. To represent the fact that ECM signaling influences Rho activation [39, 40], we assume that the basal rate of Rho activation, $b_\rho(E_k)$ is ECM-dependent.

Our models differ in the functional forms assumed for b_ρ, B_E, A_E, and L_E. We present and analyze each of these models one by one, to accentuate their differences and motivate model changes that address specific deficiencies. A summary of definitions and terms used in these models appears in Table 3 along with a complete summary of model equations in the S1 Text.

Correspondence with experiments

Parameters associated with rates of activation and/or feedback strengths are summarized in the S1 Text. The parameters γ_i represent the strengths of feedbacks 1 or 2 in Fig 2(b) and 2(c). γ_R controls the positive feedback (2) of Rac (via lamellipod spreading) on ECM signaling, and γ_ρ represents the magnitude of negative feedback (1) from Rho to ECM signaling (due to lamellipod contraction). γ_E controls the strength of ECM activation of Rho in both feedbacks (1) and (2). When these feedbacks depend on cell state variables, we typically use Hill functions with magnitude γ_i, or, occasionally, linear expressions with slopes $\bar{\gamma}_i$. (These choices are distinguished by usage of overbar to avoid confusing distinct units of the γ's in such cases.)

Experimental manipulations in [11] (described in Section "Experimental observations constraining the models") can be linked to the following parameter variations.

- ROCK inhibition treatment (O1) suppresses the link between Rho activity and actomyosin contraction. Hence this inhibition can be identified with reduction of γ_ρ.

- Invasiveness (O2) is associated with differences in both PTEN and PI3K activity (more invasive cells exhibit more PI3K and less PTEN). Increasing PI3K activity, or increasing net protrusive activity could correspond to increasing γ_R.

- Increasing fibronectin (FN) density (O3) leads to increased ECM signaling to Rac, and is thus associated with increased γ_E (or $\bar{\gamma}_E$).

- Membrane tension, cytoskeletal availability, mechanical forces, or other resource limitation in the cell can all potentially affect lamellipodial coupling. These were not perturbed experimentally but can be represented by variation of the coupling parameter l_c.

In view of this correspondence between model parameters and experimental manipulations, our subsequent analysis and bifurcation plots will highlight the role of feedback parameters $\gamma_{R,\rho,E}$ in the predictions of each model. Rather than exhaustively mapping all parameters, our goal is to use 1 and 2-parameter bifurcation plots with respect to these parameters to check for (dis)agreement between model predictions and experimental observations (O1–O3). This allows us to (in)validate several hypotheses and identify the eventual model (the Hybrid, Model 3) and set of hypotheses that best account for observations.

Lamellipod competition (Models 1)

We first investigated the possibility that lamellipod competition is responsible for bistability and that GTPases interactions create negative feedback that drives the oscillations observed in some cells. To explore this idea, we represented the interplay between lamellipodia (e.g., competition for growth due to membrane tension or volume constraints), using an elementary Lotka-Volterra (LV) competition model. For simplicity, we assume that A_E, L_E depend linearly on Rac and Rho concentration, and set $B_E = 0$. (This simplifies subsequent analysis without significantly affecting qualitative conclusions.) With these assumptions, the ECM Eq (3c) reduce to the well-known LV species-competition model.

First consider Eq (3c) as a function of parameters (A_E, L_E), in isolation from GTPase input. As in the classical LV system [45], competition gives rise to coexistence, bistability, or competitive exclusion, the latter two associated with a polarized cell. These regimes are indicated on the parameter plane of Fig 3a with the ratios of contractile (L_E) and protrusive (A_E) strengths in each lamellipod as parameters. (In the full model, these quantities depend on Rac and Rho activities; the ratios $L_E(\rho_k)/A_E(R_k)$ for lamellipod $k = 1, 2$ lead to aggregate parameters that simplify this figure.) We can interpret the four parameter regimes in Fig 3a as follows: I) a bistable regime: depending on initial conditions, either lamellipod "wins" the competition. II) Lamellipod 1 always wins. III) Lamellipod 2 always wins. IV) Lamellipods 1 and 2 coexist at finite sizes. Regimes I-III represent strongly polarized cells, whereas IV corresponds to an unpolarized (or weakly polarized) cell.

We next asked whether, and under what conditions, GTPase-mediated feedback could generate relaxation oscillations. Such dynamics could occur provided that slow negative feedback drives the ECM subsystem from an E_1-dominated state to an E_2-dominated state and back. In Fig 3a, this correspond to motion along a path similar to one labeled (d) in Panel (a), with the ECM subsystem circulating between Regimes II and III. This can be accomplished by GTPase feedback, since both Rho and Rac modulate L_E (contractile strength) and A_E (protrusion
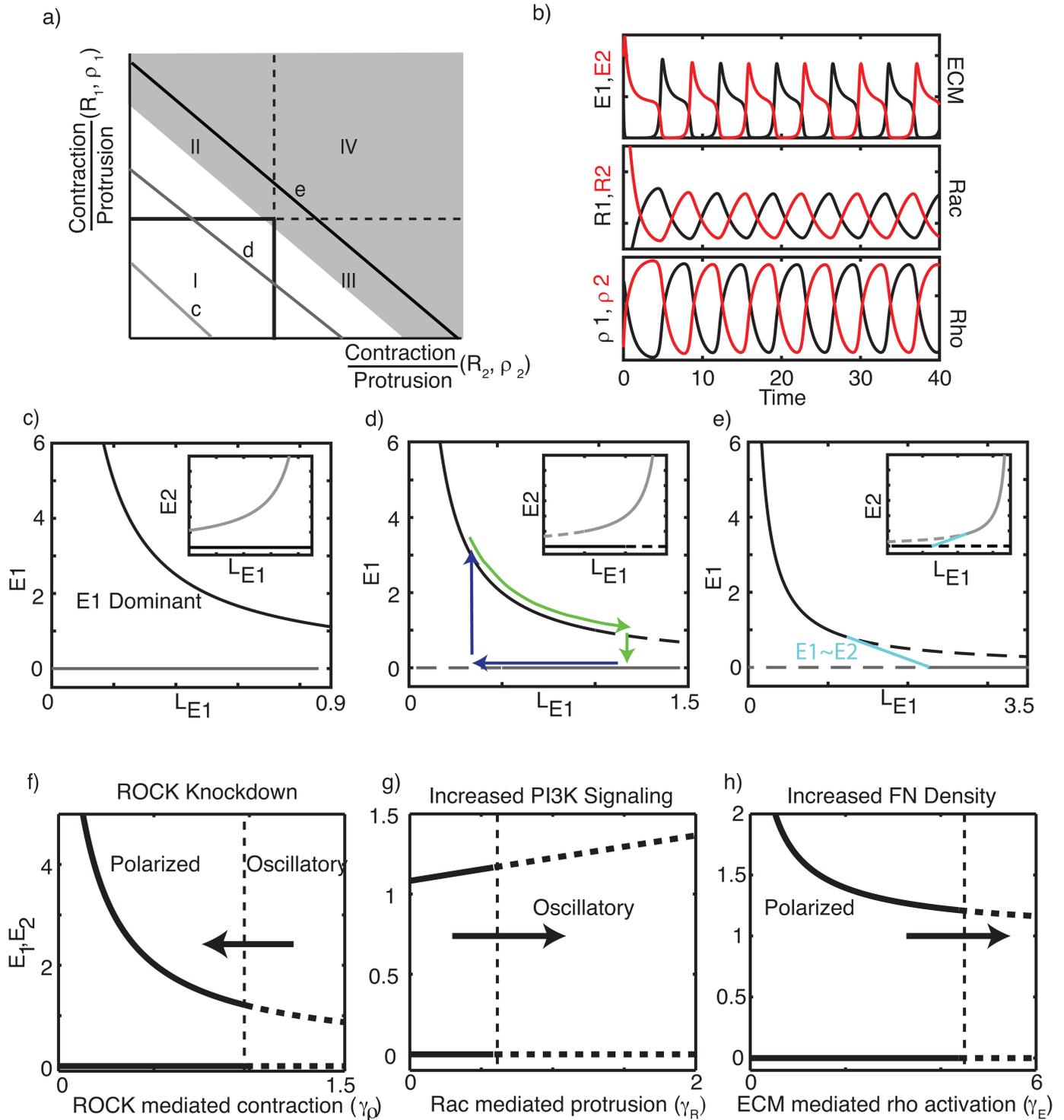
Fig 3. Lamellipod competition (Model 1). (a) On its own, the ECM signaling (lamellipod competition) submodel (Eq (3c)) with $L_E(\rho_{1,2})$ and $A_E(R_{1,2})$ taken as parameters) has four regimes. Regimes I-III: a polarized cell with a single lamellipod (bistability in I and competitive exclusion in II-III). Regime IV, lamellipods coexist. Axes represent ratios of $L_E(\rho_k)/A_E(R_k)$ for each lamellipod ($k = 1, 2$). Horizontal and vertical lines are transcritical bifurcations (at $l_c/A_E(R_k)$). **(b)** Typical simulation of Model **1b** shows temporal oscillations in ECM signaling and Rac-Rho activities. $\gamma_\rho = 1.5$ and all other parameters are as in the S1 Text. **(c-e)** One-parameter bifurcation diagrams for E_1 corresponding to the paths labeled c-e in Panel (a) (produced by tuning L_{E1} while keeping $L_{E1} + L_{E2} = K$ = constant, for K = 0.9, 1.5, 3.5). Other ECM parameters: $A_{E1} = A_{E2} = l_c = 1$. Insets show E_2 levels. Cycles of protrusion (green) and contraction (blue), shown in panel (d), can occur when feedback from GTPases tunes the relative contraction parameter L_{E1} or L_{E2}. **(f-h)** Bifurcation

diagrams linking predicted behavior to experimental perturbations. Panel title represents the direction of the arrow on each panel. Thick curves: stable polar solutions (solid) and oscillations (dashed). Vertical lines represent Hopf bifurcations. Parameters are as in the S1 Text.

strength). We show this idea more explicitly in Fig 3(c)–3(e) by plotting E_1 vs L_{E1} while keeping $L_{E1} + L_{E2}$ constant. (Insets similarly show E_2 vs L_{E1}.) Each of Panels (c-e) corresponds to a 1-parameter bifurcation plot along the corresponding path labeled (c-e) in Panel (a). We find the following possible transitions: In Fig 3c, we find two distinct polarity states: either E_1 or E_2 dominate while the other is zero regardless of the value of L_{E1}; a transition between such states does not occur. In Fig 3d, there is a range of values of L_{E1} with coexisting stable low and high E_1 values (bistable regime) flanked by regimes where either the lower or higher state loses stability (monostable regimes). As indicated by the superimposed loop, a cycle of protrusion (green) and contraction (blue) could then generate a relaxation oscillation as the system traverses its bistable regime. In Fig 3e, a third possibility is that the system transits between E₁-dominated, coexisting, and E₂-dominated states. In brief, for oscillatory behavior, GTPase feedback should drive the ECM-subsystem between regimes I, II, and III without entering regime IV.

Informed by this analysis, we next link the bistable ECM submodel to a Rac-Rho system. To ensure that the primary source of bistability is ECM dynamics, a monostable version of the Rac-Rho sub-system is adopted by setting $n = 1$ in the GTPase activation terms A_R, A_ρ in Eqs (3a) and (3b). We consider three possible model variants (1a-1c) for the full ECM / GTPase model.

Abundant GTPases (Model 1a). We first assume that both Rac and Rho are abundant (R_I, ρ_I taken to be constant). Coupling the GTPase and ECM layers introduces temporal dependence in the parameters A_E, L_E (and thus in the ratios of contraction/protrusion for the lamellipods that form the axes in Fig 3a). Consequently, a point representing the cell on this figure would drift from one regime to another as the dynamics evolve. In this way, the dynamics of the system as a whole is analyzed from the standpoint of how the GTPase-ECM feedbacks drive the ECM subsystem between its distinct regimes. It follows that oscillating cells are represented by a trajectory that cycles between regimes II and III where the cell would be polarized in opposite directions.

While in principle, such cycles seem plausible, in practice, we were unable to find them despite reasonable parameter space exploration. (We do not entirely rule out this model, in absence of an exhaustive parameter space exploration and adjustment of all possible kinetic terms.) Based on our extensive simulations, however, we speculate that oscillations fail for one of two reasons.

- When the maximum contractile strength is low (max $L_E < l_c$, which would result from small γ_ρ), it is mathematically impossible for the system to exit Regime I (the border of this regime occurs at $L_E = l_c$). Thus oscillations are not possible since the system cannot enter regions II or III. In this case polarity is possible but not oscillations.

- When stronger contractile strength is allowed (max $L_E > l_c$, which would result from larger γ_ρ), the system still does not oscillate. Instead of traversing Regime I, the system crosses into Regime IV. Once in this regime, the apolar solution stabilizes and no oscillation ensues.

As we show next, a small, biologically motivated adjustment discussed in Model variant 1b easily promotes oscillations.

Limited (conserved) GTPases (Model 1b). We next asked how a limited total amount of each GTPase would influence model dynamics. This idea rests on our previous experience

with GTPase models in which conservation of the total amount of GTPase played an important role [27, 29–32, 46–49]. To address this question, we augmented Model 1 (Eq (3)), with the additional assumption of GTPase conservation Eq (1b).

Conservation introduces a pair of linear algebraic equations of the form $\rho_1 + \rho_2 + \rho_I = \rho_T$ (and similarly for R). Since $L_E(\rho_{1,2})$ depend linearly on ρ in this model variant (Table 3), this places a restriction on the sum $L_E(\rho_1) + L_E(\rho_2)$. As a result, part of the parameter space in Fig 3a becomes inaccessible (schematically represented in gray) so that the model becomes restricted to the white region. While $L_E(\rho_{1,2})$ could each individually exceed the coupling strength (l_c) (required for oscillations), the system as a whole is unable to access Region IV. In principle, this corrects both issues that led to failure of oscillations in Model 1a, so that slow negative feedback that modulates $L_E(\rho_{1,2})$ should then generate relaxation oscillations. With this adjustment, we indeed found wide parameter regimes corresponding to oscillations (see Fig 3b for an example).

We next evaluated this model against experimental observations (O1–O3). First, the model predicts that ROCK inhibition suppresses oscillations (Fig 3a) while increased fibronectin promotes oscillations (Fig 3c), in agreement with (O1) and (O3). Second, increased PI3K (or reduced PTEN which acts as a PI3K antagonist) is linked to Rac-mediated protrusion (Section "Correspondence with experiments"). This increases the strength of Feedback 2 and promotes oscillations (Fig 3b). Given the link between PTEN suppression / elevation of PI3K in invasive cells, this is consistent with O2.

While this model can account for all three observations, one significant issue leads us to reject it. The timescales required to generate oscillations in this model are inconsistent with known biological timescales. Relaxation oscillators require that a *slow* variable provides the negative feedback that promotes oscillations. Since Model 1 is predicated on negative feedback from GTPases to bistable ECM-cell contact area subsystem, it implies that GTPase dynamics must occur on a slower time scale than that of the cell-ECM subsystem. This appears to be unreasonable based on the fact that GTPase activation/inactivation operates on a typical time-scale of seconds, much faster than the actomyosin-based protrusion and contraction of cells. Indeed, when GTPase dynamics are faster than ECM dynamics ($\epsilon < 1$), oscillations no longer occur. For this reason, we reject Model 1b as it stands.

GTPase effectors (Model 1c). Before dismissing Model 1 on grounds of timescale, we considered one additional modification. We asked whether the fast timescale of GTPases could be retarded by downstream effectors that participate in relevant feedback loops. To study this possibility, we supplemented Eqs (3) and (1b) with dynamics of intermediate Rac effectors $w_{1,2}$ (e.g. WASP, WAVE, PI3K, or other downstream components) and Rho effectors $c_{1,2}$ (e.g. ROCK, etc.) that could correct the timescale problem. These putative effectors are represented as simple dynamic variables (See Figure A in S1 Text), with the parameter ϵ_2 governing timescale. In the $\epsilon_2 \gg \epsilon$ limit, this variant reduces (by a quasi steady state approximation) to Model 1b.

The structure of Model 1c and the number and values of steady states are the same as in Model 1b. Only the timescales associated with various model components change. This model could hence account for the same experimental observations as Model 1b. Further, if $\epsilon_2 < \epsilon < 1$, it can do so with GTPase dynamics faster than ECM dynamics. Unfortunately, while GTPase dynamics no longer need be slow, dynamics of ROCK / WASP must be slower than ECM dynamics, which is still biologically implausible.

To summarize, we have grounds for rejecting a model in which ECM dynamics are central to the generation of bistability and polarity. To achieve oscillations with such a model, other components of the system must operate on a slow timescale. Biologically, since GTPases and their effectors regulate protrusion and contraction, it is only reasonable that they operate on a

faster timescale than lamellipodial dynamics, and cannot therefore be the source of slow negative feedback. This motivates the development of our next attempt in which we reverse the roles of GTPases and ECM as sources of bistability and negative feedback.

Bistable GTPases (Model 2)

In view of the conclusions thus far, we now explore the possibility that bistability stems from mutual antagonism between Rac and Rho, rather than lamellipod competition. To do so, we chose Hill coefficients $n = 3$ in the rates of GTPase activation, A_R, A_ρ. We then assume that ECM signaling both couples the lamellipods and provides the requisite slow negative feedback. Here we consider the case that GTPases are abundant, so that the levels of inactive Rac and Rho (R_I, ρ_I) are constant.

We first characterize the GTPase dynamics with $b_{R,\rho}$ as parameters. Subsequently, we include ECM signaling dynamics and determine how the feedback drives the dynamics in the (b_R, b_ρ) parameter plane.

Isolated from the ECM influence, each lamellipod is independent so we only consider the properties of GTPase signaling in one. This mutually antagonistic GTPase submodel is the well-known "toggle switch" [50] that has a bistable regime, as shown in the (b_R, b_ρ) plane of Fig 4a. ECM signaling affects the Rac / Rho system only as an input to b_ρ. A linear dependence of b_ρ on E_k failed to produce an oscillatory parameter regime, so we used a nonlinear Hill type dependence with basal and saturating components. Furthermore, for GTPase influence on ECM signaling we use Hill functions for the influence of Rho (in L_E) and Rac (in B_E) on protrusion and contraction. We set $A_E = 0$ in this model for simplicity. (Nonzero A_E can lead to compounded ECM bistability that we here do not consider.)

Given the structure of the $b_\rho - b_R$ parameter plane and the fact that ECM signaling variables only influence b_ρ, we can view oscillations as periodic cycles of contraction and protrusion forming a trajectory along one of horizontal dashed lines in Fig 4a. This idea guides our
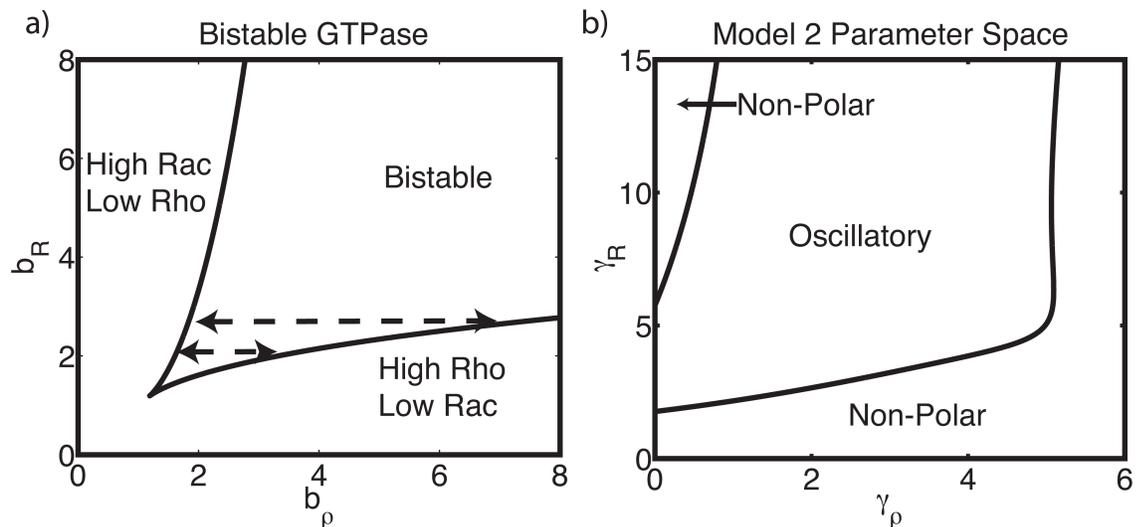

Fig 4. Bistable GTPases mode (Model 1). (a) Bifurcation analysis of Eqs (3a) and (3b) with respect to GTPase activation rate parameters b_R and b_ρ (here assumed fixed, independent of E_k to decouple the ECM module). Other parameters: $n = 3$, $\delta = 1$. Dashed lines indicate the bistable range of b_ρ values that must be traversed to induce oscillation. Compare to Fig 5a. **(b)** Bifurcation analysis of Model **2** with respect to the strength of the feedbacks γ_R and γ_ρ. Two curves of Hopf bifurcations separate oscillatory and static (but non-polar) regimes of behavior. Parameters values are provided in S1 Text.

https://doi.org/10.1371/journal.pcbi.1005524.g004

parametrization of the model. We select a value of b_R that admits a bistable range of b_ρ in Fig 4a. Next we choose maximal and minimal values of the function $b_\rho(E_K)$ that extend beyond the borders of the bistable range. This choice means that the system transitions from the high Rac / low Rho state to the low Rac / high Rho state over each of the cycles of its oscillation. With this parametrization, we find oscillatory dynamics, as shown in Fig 4b.

We now consider the two-lamellipod system with the above GTPase module in each lamellipod; we challenge the full model with experimental observations. Since each lamellipod has a unique copy of the Rac-Rho module, ECM signaling provides the only coupling between the two lamellipods. First, we observed that inhibition of ROCK (reduction of γ_ρ in Fig 4b) suppress oscillations. However the resulting stationary state is non-polar, in contrast to experimentally observed increase in the fraction of polarized cells (O1). We adjusted the coupling strength (l_c) to ensure that this disagreement was not merely due to insufficient coupling between the two lamellipods. While an oscillatory regime persists, the discrepancy with (O1) is not resolved: the system oscillates, but inhibiting ROCK gives rise to a non-polarized stationary state, contrary to experimental observations.

Yet another problematic feature of the model is its undue sensitivity to the strength of Rac activation (b_R). This is evident from a comparison of the dashed lines in Fig 4a. A small change in b_R (vertical shift) dramatically increases the range of bistability (horizontal span), and hence the range of values of b_ρ to be traversed in driving oscillations. This degree of sensitivity seems inconsistent with biological behavior.

It is possible that an alternate formulation of the model (different kinetic terms or different parametrization) might fix the discrepancies noted above, so we avoid ruling out this scenario altogether. In our hands, this model variant failed. However a simple augmentation, described below, addresses all deficiencies, and leads to the final result.

Hybrid (Model 3)

In our third and final step, we add a small but significant feature to the bistable GTPase model to arrive at a working variant that accounts for all observations. Keeping all equations of Model 2, we merely drop the assumption of unlimited Rac and Rho. We now require that the total amount of each GTPase be conserved in the cell. This new feature has two consequences. First, lamellipods now compete not only for growth, but also for limited pools of Rac and Rho. This, along with rapid diffusion of inactive GTPases across the cell [30, 31, 51] provides an additional global coupling of the two lamellipods. This seemingly minor revision produces novel behavior.

We proceed as before, first analyzing the GTPase signaling system on its own. With conservation, the $b_R - b_\rho$ plane has changed from its previous version (Fig 4a for Model 2) to Fig 5a. For appropriate values of b_R, there is a significant bistable regime in b_ρ. Indeed, we find three regimes of behavior as the contractile strength in lamellipod k, $b_\rho(E_k)$, varies: a bistable regime where polarity in either direction is possible, a regime where lamellipod j "wins" ($E_j > E_k$, left of the bistable regime), and a regime where lamellipod k "wins" (right of the bistable regime). Only polarity in a single direction is possible on either side of the bistable regime.

As in Model 2, we view oscillations in the full model as cycles of lamellipodial protrusion and contraction that modify $b_\rho(E_k)$ over time, and result in transitions between the three polarity states. To parameterize the model, we repeat the process previously described (choose a value of b_R consistent with bistability, then choose the dependence of b_ρ on ECM signaling so as to traverse that entire bistable regime.)

We couple the GTPase system with ECM equations as before. We then check for agreement with observations (O1–O3). As shown in Fig 5(e) and 5(f), the model produces both polarized
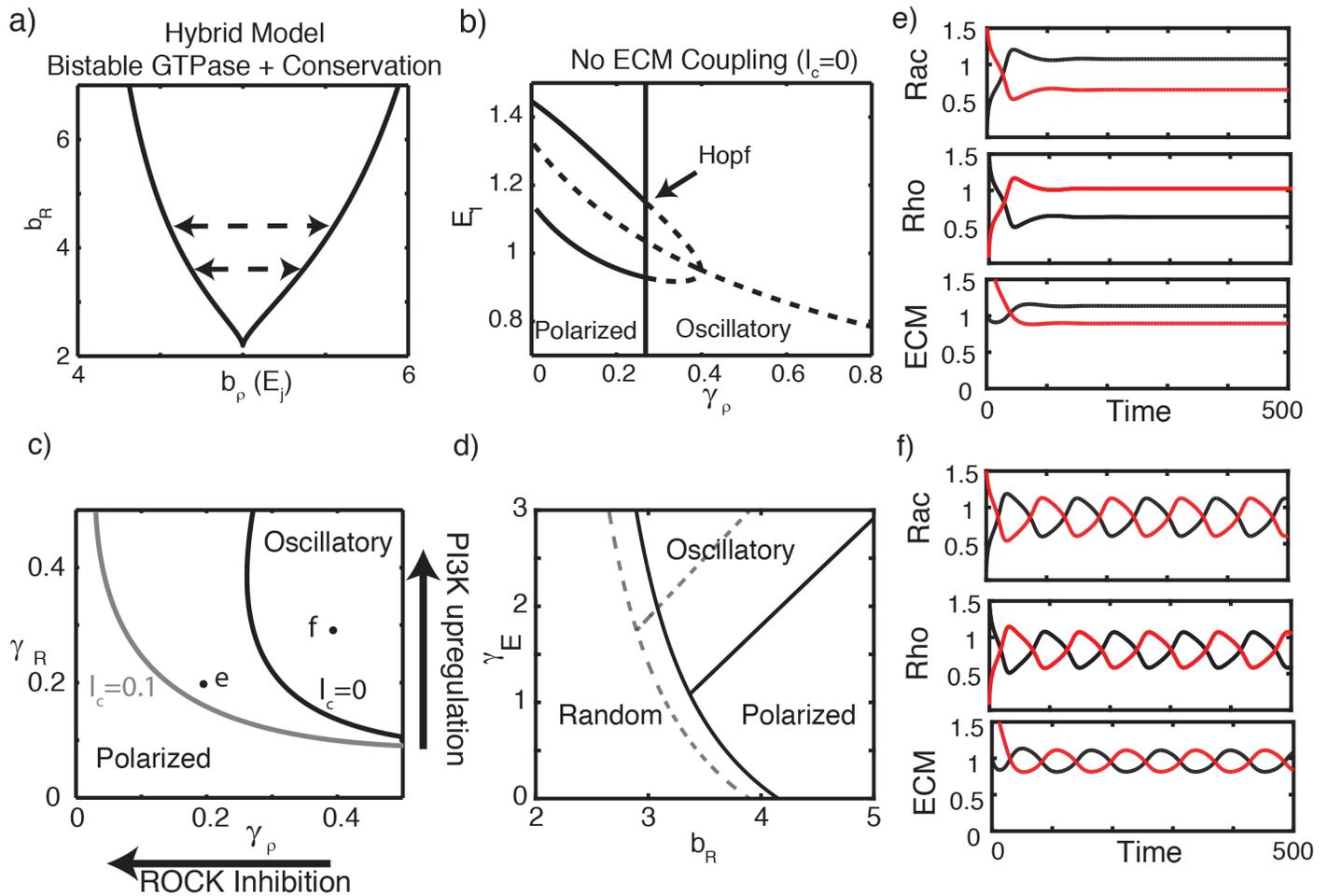
Fig 5. Hybrid Model (Model 3). Assuming that the pools of Rac and Rho are constant in the cell fixes undesirable features of Model 2. **(a)** As in Fig 4(a) but with GTPase conservation Eq (1b). Other parameters: $n = 3$, $\delta = 1$, $\rho_T = R_T = 2$. Dashed lines indicate the range of b_ρ values that must be traversed to induce oscillation. **(b)** Bifurcation analysis with respect to γ_ρ. Polarized (indicated by stable steady states, solid curves) and oscillatory (unstable steady states, dashed curves) regimes are present. **(c)** Two-parameter bifurcation diagrams depicting oscillatory and polarized parameter regimes separated by a locus of Hopf bifurcations, both with ($l_c = 0.1$) and without ($l_c = 0$) direct lamellipod coupling. Points (e,f) indicate parameter values at which simulations were performed (with $l_c = 0$) to confirm dynamics. **(d)** Bifurcation diagram of the full model, with respect to basal Rac activation rate b_R and ECM-induced Rho activation rate γ_E, concordant with such diagrams in [11]. Solid (respectively dashed) lines indicate the boundary of different dynamical regimes without (resp. with) feedback from ECM onto Rac activation. **(e,f)** Sample simulations showing lamellipodial polarity and oscillations (ECM signaling levels in each lamellipod over time). Parameter values correspond to the labeled points in panel (c). For (e), $l_c = 0$, $\gamma_R = 0.2$, $\gamma_\rho = 0.2$. For (f), $l_c = 0$, $\gamma_R = 0.3$, $\gamma_\rho = 0.4$. All other parameters are given in the S1 Text.

https://doi.org/10.1371/journal.pcbi.1005524.g005

and oscillatory solutions. To check consistency with experiments, we mapped the dynamics of this model with respect to both ROCK mediated contraction and PI3K mediated protrusion (Fig 5c). Inhibiting ROCK (Fig 5b, decreasing γ_ρ) results in a transition from oscillations to polarized states, consistent with (O1). PI3K upregulation promotes oscillations (increasing γ_R, Fig 5c), characteristic of the more invasive cell line 1205Lu (consistent with O2). Finally, increased fibronectin density (increased γ_E, Fig 5d) also promotes oscillations, consistent with (O3). We conclude that this Hybrid Model can account for polarity and oscillations, and that it is consistent with the three primary experimental observations (O1–3). Finally, Model 3 can recapitulate such observations with more reasonable timescales for GTPase and ECM dynamics than were required for Model variant 1b.

It is apparent that Model 3 contains two forms of lamellipodial coupling: direct (mechanical) competition and competition for the limited pools of inactive Rac and Rho. While the former is certain to be an important coupling in some contexts or conditions [52], we find that it is dispensable in this model (e.g, see $l_c = 0$ in Fig 5c). We comment about the effect of such coupling in the Discussion. In the context of this final model, we also tested the effect of ECM activation of Rac (in addition to the already assumed effect on Rho activation). As shown in Fig 5d (dashed curves), the essential bifurcation structure is preserved when this modification is incorporated (details in the S1 Text, and implications in the Discussion).

Summary of results

To summarize, Model 1b was capable of accounting for all observations, but required conservation of GTPase to do so. This model was however rejected due to unreasonable time scales needed to give rise to oscillations. Model 2 could account for oscillations with appropriate timescales, but it appears to be highly sensitive to parameters and, in our hands, inconsistent with experimental observations. Model 3, which combines the central features of Models 1b and 2, has the right mix of timescales, and agrees with experimental observations. In that final Hybrid Model, ECM based coupling (l_c) due to mechanical tension or competition for other resources is not essential, but its inclusion makes oscillations more prevalent (Fig 5b and 5e).

Furthermore, in this Hybrid Model, we identify two possible negative feedback motifs, shown in Fig 2b. These appear to work cooperatively in promoting oscillations. As we have argued, feedbacks are tuned so that ECM signaling spans a range large enough that $b_\rho(E_k)$ traverses the entire bistable regime (Fig 5a). This is a requirement for the relaxation oscillations schematically depicted in Fig 2c. Within an appropriate set of model parameters, either feedback could, in principle, accomplish this. Hence, if Feedback 1 is sufficiently strong, Feedback 2 is superfluous and vice versa. Alternatively, if neither suffices on its own, the combination of both could be sufficient to give rise to oscillations. Heterogeneity among these parameters could thus be responsible for the fact that in ROCK inhibition experiments (where Feedback 1 is essentially removed), most but not all cells transition to the persistent polarity phenotype.

The Hybrid Model (Model 3) is consistent with observations O1–O3. We can now challenge it with several further experimental tests. In particular, we make two predictions.

(P1). In the model, reducing the rate of Rac-mediated protrusion (γ_R) promotes persistent polarization over oscillation (Fig 5e and 5f). One way to test this experimentally is to inhibit Rac activity. Rac inhibition experiments are reported in [11], which validate the prediction: oscillations are suppressed in favor of persistent polarization.

(P2). Alternatively, the Hybrid model predicts that promoting Rho-mediated contraction (increasing γ_ρ) promotes oscillations over persistent polarization. This was tested in [11] by ablating microtubules. Previously, it was found that the application of nocodazole, which breaks up microtubules (MTs), leads to the release of MT-sequestered Rho-GEF (GEF-H1) which subsequently activates Rho and promotes contraction [53]. Experiments of this type are reported in [2], where cells were constrained to move in 1D by micropatterned adhesive strips. In experiments by [11] it was indeed shown that MT suppression promotes oscillation, consistent with this model prediction.

Discussion

Migrating cells can exhibit a variety of behaviors. These behaviors can be modulated by the cell's internal state, its interactions with the environment, or mutations such as those leading

to cancer progression. In most cases, the details of mechanisms underlying a specific behavior, or leading to transitions from one phenotype to another are unknown or poorly understood. Moreover, even in cases where one or more defective proteins or genes are known, the complexity of signaling networks make it difficult to untangle the consequences. Hence, using indirect observations of cell migration phenotypes to elucidate the properties of underlying signaling modules and feedbacks are, as argued here, a useful exercise.

Using a sequence of models and experimental observations (O1–O3) we tested several plausible hypotheses for melanoma cell migration phenotypes observed in [11]. By so doing, we found that GTPase dynamics are fundamental to providing 1) bistability associated with polarity and 2) coupling between competing lamellipods to select a single "front" and "rear". (This coupling is responsible for the antiphase lamellipodial oscillations). Further, slow feedback between GTPase and ECM signaling resulting from contraction and protrusion generate oscillations similar those observed experimentally.

The single successful model, Hybrid Model (Model 3), is essentially a relaxation oscillator. Mutual inhibition between the limited pools of Rac and Rho, sets up a primary competition between lamellipods that produces a bistable system with polarized states pointing in opposite directions. Interactions between GTPase dynamics and ECM signaling provide the negative feedback required to flip this system between the two polarity states, generating oscillations for appropriate parameters. Results of Model 3 are consistent with observations (O1–O3), and lead to predictions (P1–P2), that are also confirmed by experimental observations [11]. In [11], it is further shown that the fraction of cells exhibiting each of these behaviors can be quantitatively linked to heterogeneity in the ranges of parameters representing the cell populations in the model's parameter space.

In our models, we assumed that the dominant effect of ECM signaling input is to activate Rho, rather than Rac. In reality, both GTPases are likely activated to some extent in a cell and environment-dependent manner [41, 42]. We can incorporate ECM activation of Rac by amending the term A_R so that its magnitude is dependent on ECM signaling (E_k). Doing so results in a shift in the borders of regimes we have indicated in Fig 5d (dashed versus solid borders, see S1 Text for more details). So long as Rho activation is the dominant effect, this hardly changes the qualitative results. As the strength of feedback onto Rac strengthens, however, the size of the oscillatory regime is reduced. Thus if feedback onto Rac dominates, loss of oscillations would be predicted. This is to be expected based on the structure of these interactions. Where ECM → Rho mediates a negative feedback, ECM → Rac mediates a positive feedback, which would be expected to suppress oscillatory behavior. Thus while the ECM likely mediates multiple signaling feedbacks, this modeling suggest feedback onto Rho is most consistent with observations.

We have argued that conservation laws (fixed total amount of Rac and fixed total amount of Rho) in the cell plays an important role in the competition between lamellipods. Such conservation laws are also found to be important in a number of other settings. Fully spatial (PDE) modeling of GTPase function has shown that conservation significantly alters signaling dynamics [27, 31, 54]. In [55], it was shown that stochastically initiated hot spots of PI3K appeared to be globally coupled, potentially through a shared and conserved cytoplasmic pool of a signaling regulator. Conservation of MIN proteins, which set up a standing wave oscillation during bacterial cell division, has been shown to give rise to a new type of Turing instability [56]. Finally, interactions between conserved GTPase and negative regulation from F-actin in a PDE model was shown to give rise to a new type of conservative excitable dynamics [46, 47], which have been linked to the propagation of actin waves [57].

These results provide interesting insights into the biology of invasive cancer cells (in melanoma in particular), and shed light onto the mechanisms underlying the extracellular matrix-

induced polarization and migration of normal cells. First, they illustrate that diverse polarity and migration patterns can be captured within the same modeling framework, laying the foundation for a better understanding of seemingly unrelated and diverse behaviors previously reported. Second, our results present a mathematical and computational platform that distills the critical aspects and molecular regulators in a complex signaling cascade; this platform could be used to identify promising single molecule and molecular network targets for possible clinical intervention.

Supporting information

S1 Text. Supplemental text containing full equations for all models along with parameters and a description of how parameters were obtained.
(PDF)

Author Contributions

Conceptualization: WRH AL LEK.

Formal analysis: WRH.

Funding acquisition: WRH AL LEK.

Methodology: WRH LEK.

Project administration: WRH LEK.

Software: WRH.

Supervision: AL LEK.

Writing – original draft: WRH JP AL LEK.

References

1. Camley BA, Zhao Y, Li B, Levine H, Rappel WJ (2013) Periodic migration in a physical model of cells on micropatterns. Physical review letters 111: 158102. https://doi.org/10.1103/PhysRevLett.111.158102 PMID: 24160631

2. Zhang J, Guo WH, Wang YL (2014) Microtubules stabilize cell polarity by localizing rear signals. Proceedings of the National Academy of Sciences 111: 16383–16388. https://doi.org/10.1073/pnas.1410533111

3. Fraley SI, Feng Y, Giri A, Longmore GD, Wirtz D (2012) Dimensional and temporal controls of three-dimensional cell migration by zyxin and binding partners. Nature communications 3: 719. https://doi.org/10.1038/ncomms1711 PMID: 22395610

4. Maiuri P, Rupprecht JF, Wieser S, Ruprecht V, Bénichou O, et al. (2015) Actin flows mediate a universal coupling between cell speed and cell persistence. Cell 161: 374–386. https://doi.org/10.1016/j.cell.2015.01.056 PMID: 25799384

5. Lavi I, Piel M, Lennon-Dumenil AM, Voituriez R, Gov NS (2016) Deterministic patterns in cell motility. Nat Phys 12: –. https://doi.org/10.1038/nphys3836

6. Shao D, Levine H, Rappel WJ (2012) Coupling actin flow, adhesion, and morphology in a computational cell motility model. Proceedings of the National Academy of Sciences 109: 6851–6856. https://doi.org/10.1073/pnas.1203252109

7. Vellinga T, den Uil S, Rinkes I, Marvin D, Ponsioen B, et al. (2016) Collagen-rich stroma in aggressive colon tumors induces mesenchymal gene expression and tumor cell invasion. Oncogene. https://doi.org/10.1038/onc.2016.60 PMID: 26996663

8. Provenzano PP, Eliceiri KW, Campbell JM, Inman DR, White JG, et al. (2006) Collagen reorganization at the tumor-stromal interface facilitates local invasion. BMC medicine 4: 1. https://doi.org/10.1186/1741-7015-4-38

9. Balcioglu HE, van de Water B, Danen EH (2016) Tumor-induced remote ECM network orientation steers angiogenesis. Scientific reports 6. https://doi.org/10.1038/srep22580

10. Park J, Kim DH, Kim HN, Wang CJ, Kwak MK, et al. (2016) Directed migration of cancer cells guided by the graded texture of the underlying matrix. Nature materials. https://doi.org/10.1038/nmat4586

11. Park J, Holmes WR, Lee SH, Kim HN, Kim DH, et al. (2017) A mechano-chemical feedback underlies co-existence of qualitatively distinct cell polarity patterns within diverse cell populations. arXiv:161208948v1.

12. Holmes WR, Edelstein-Keshet L (2012) A comparison of computational models for eukaryotic cell shape and motility. PLoS Comput Biol 8: e1002793. https://doi.org/10.1371/journal.pcbi.1002793 PMID: 23300403

13. Miller AJ, Mihm MC Jr (2006) Melanoma. New England Journal of Medicine 355: 51–65. https://doi.org/10.1056/NEJMra052166 PMID: 16822996

14. Haass NK, Smalley KS, Li L, Herlyn M (2005) Adhesion, migration and communication in melanocytes and melanoma. Pigment cell research 18: 150–159. https://doi.org/10.1111/j.1600-0749.2005.00235.x PMID: 15892711

15. Ridley AJ (2001) Rho family proteins: coordinating cell responses. Trends in cell biology 11: 471–477. https://doi.org/10.1016/S0962-8924(01)02153-5 PMID: 11719051

16. Ridley AJ, Schwartz MA, Burridge K, Firtel RA, Ginsberg MH, et al. (2003) Cell migration: Integrating signals from front to back. Science 302: 1704–1709. https://doi.org/10.1126/science.1092053 PMID: 14657486

17. Devreotes P, Horwitz AR (2015) Signaling networks that regulate cell migration. Cold Spring Harbor perspectives in biology 7: a005959. https://doi.org/10.1101/cshperspect.a005959 PMID: 26238352

18. Guilluy C, Garcia-Mata R, Burridge K (2011) Rho protein crosstalk: another social network? Trends in cell biology 21: 718–726. https://doi.org/10.1016/j.tcb.2011.08.002 PMID: 21924908

19. Byrne KM, Monsefi N, Dawson JC, Degasperi A, Bukowski-Wills JC, et al. (2016) Bistability in the Rac1, PAK and RhoA signalling network is a feature of cell motility. Cell Systems 2: 38–48. https://doi.org/10.1016/j.cels.2016.01.003 PMID: 27136688

20. Maekawa M, Ishizaki T, Boku S, Watanabe N, Fujita A, et al. (1999) Signaling from Rho to the actin cytoskeleton through protein kinases ROCK and LIM-kinase. Science 285: 895–898. https://doi.org/10.1126/science.285.5429.895 PMID: 10436159

21. Parri M, Chiarugi P (2010) Rac and Rho GTPases in cancer cell motility control. Cell Commun Signal 8: 10–1186. https://doi.org/10.1186/1478-811X-8-23

22. Sailem H, Bousgouni V, Cooper S, Bakal C (2014) Cross-talk between Rho and Rac GTPases drives deterministic exploration of cellular shape space and morphological heterogeneity. Open biology 4: 130132. https://doi.org/10.1098/rsob.130132 PMID: 24451547

23. Symons M, Segall JE (2009) Rac and Rho driving tumor invasion: who's at the wheel. Genome Biol 10: 213. https://doi.org/10.1186/gb-2009-10-3-213 PMID: 19291272

24. Holmes WR, Lin B, Levchenko A, Edelstein-Keshet L (2012) Modelling cell polarization driven by synthetic spatially graded Rac activation. PLoS Comput Biol 8: e1002366. https://doi.org/10.1371/journal.pcbi.1002366 PMID: 22737059

25. Lin B, Holmes WR, Wang J, Ueno T, Harwell A, et al. (2012) Synthetic spatially graded Rac activation drives directed cell polarization and locomotion. PNAS 109: E3668–E3677.

26. Huang B, Lu M, Jolly MK, Tsarfaty I, Onuchic J, et al. (2014) The three-way switch operation of Rac1/RhoA GTPase-based circuit controlling amoeboid-hybrid-mesenchymal transition. Scientific reports 4.

27. Holmes WR, Edelstein-Keshet L (2016) Analysis of a minimal Rho-GTPase circuit regulating cell shape. Physical Biology 13: 046001. https://doi.org/10.1088/1478-3975/13/4/046001 PMID: 27434017

28. Lawson CD, Burridge K (2014) The on-off relationship of Rho and Rac during integrin-mediated adhesion and cell migration. Small GTPases 5: e27958. https://doi.org/10.4161/sgtp.27958 PMID: 24607953

29. Marée AF, Jilkine A, Dawes A, Grieneisen VA, Edelstein-Keshet L (2006) Polarization and movement of keratocytes: A multiscale modelling approach. Bull Math Biol 68: 1169–1211. https://doi.org/10.1007/s11538-006-9131-7 PMID: 16794915

30. Jilkine A, Marée AF, Edelstein-Keshet L (2007) Mathematical model for spatial segregation of the Rho-Family GTPases based on inhibitory crosstalk. Bull Math Biol 69: 1943–1978. https://doi.org/10.1007/s11538-007-9200-6 PMID: 17457653

31. Mori Y, Jilkine A, Edelstein-Keshet L (2008) Wave-pinning and cell polarity from a bistable reaction-diffusion system. Biophys J 94: 3684–3697. https://doi.org/10.1529/biophysj.107.120824 PMID: 18212014

32. Edelstein-Keshet L, Holmes WR, Zajac M, Dutot M (2013) From simple to detailed models for cell polarization. Philosophical Transactions of the Royal Society B: Biological Sciences 368: 20130003. https://doi.org/10.1098/rstb.2013.0003

33. Gauthier NC, Fardin MA, Roca-Cusachs P, Sheetz MP (2011) Temporary increase in plasma membrane tension coordinates the activation of exocytosis and contraction during cell spreading. Proceedings of the National Academy of Sciences 108: 14467–14472. https://doi.org/10.1073/pnas.1105845108

34. Raucher D, Sheetz MP (2000) Cell spreading and lamellipodial extension rate is regulated by membrane tension. The Journal of cell biology 148: 127–136. https://doi.org/10.1083/jcb.148.1.127 PMID: 10629223

35. Tsyganov MA, Kolch W, Kholodenko BN (2012) The topology design principles that determine the spatiotemporal dynamics of G-protein cascades. Molecular BioSystems 8: 730–743. https://doi.org/10.1039/c2mb05375f PMID: 22218529

36. Weiger MC, Wang CC, Krajcovic M, Melvin AT, Rhoden JJ, et al. (2009) Spontaneous phosphoinositide 3-kinase signaling dynamics drive spreading and random migration of fibroblasts. Journal of cell science 122: 313–323. https://doi.org/10.1242/jcs.037564 PMID: 19126672

37. Bakal C, Aach J, Church G, Perrimon N (2007) Quantitative morphological signatures define local signaling networks regulating cell morphology. science 316: 1753–1756. https://doi.org/10.1126/science.1140324 PMID: 17588932

38. Cooper S, Sadok A, Bousgouni V, Bakal C (2015) Apolar and polar transitions drive the conversion between amoeboid and mesenchymal shapes in melanoma cells. Molecular biology of the cell 26: 4163–4170. https://doi.org/10.1091/mbc.E15-06-0382 PMID: 26310441

39. Danen EH, Sonneveld P, Brakebusch C, Fässler R, Sonnenberg A (2002) The fibronectin-binding integrins $\alpha 5\beta 1$ and $\alpha v\beta 3$ differentially modulate RhoA–GTP loading, organization of cell matrix adhesions, and fibronectin fibrillogenesis. The Journal of cell biology 159: 1071–1086. https://doi.org/10.1083/jcb.200205014 PMID: 12486108

40. Park JH, Ryu JM, Han HJ (2011) Involvement of caveolin-1 in fibronectin-induced mouse embryonic stem cell proliferation: Role of FAK, RhoA, PI3K/Akt, and ERK 1/2 pathways. Journal of cellular physiology 226: 267–275. https://doi.org/10.1002/jcp.22338 PMID: 20658539

41. Arthur WT, Petch LA, Burridge K (2000) Integrin engagement suppresses RhoA activity via a c-Src-dependent mechanism. Current Biology 10: 719–722. https://doi.org/10.1016/S0960-9822(00)00537-6 PMID: 10873807

42. Costa P, Scales TM, Ivaska J, Parsons M (2013) Integrin-specific control of focal adhesion kinase and rhoa regulates membrane protrusion and invasion. PLoS One 8: e74659. https://doi.org/10.1371/journal.pone.0074659 PMID: 24040310

43. Novák B, Tyson JJ (2008) Design principles of biochemical oscillators. Nature reviews Molecular cell biology 9: 981–991. https://doi.org/10.1038/nrm2530 PMID: 18971947

44. Markevich NI, Hoek JB, Kholodenko BN (2004) Signaling switches and bistability arising from multisite phosphorylation in protein kinase cascades. The Journal of cell biology 164: 353–359. https://doi.org/10.1083/jcb.200308060 PMID: 14744999

45. Edelstein-Keshet L (1988) Mathematical models in biology, volume 46 of *Classics in Applied Mathematics*. SIAM.

46. Holmes W, Carlsson A, Edelstein-Keshet L (2012) Regimes of wave type patterning driven by refractory actin feedback: transition from static polarization to dynamic wave behaviour. Physical biology 9: 046005. https://doi.org/10.1088/1478-3975/9/4/046005 PMID: 22785332

47. Mata MA, Dutot M, Edelstein-Keshet L, Holmes WR (2013) A model for intracellular actin waves explored by nonlinear local perturbation analysis. Journal of theoretical biology 334: 149–161. https://doi.org/10.1016/j.jtbi.2013.06.020 PMID: 23831272

48. Holmes WR (2014) An efficient, nonlinear stability analysis for detecting pattern formation in reaction diffusion systems. Bulletin of mathematical biology 76: 157–183. https://doi.org/10.1007/s11538-013-9914-6 PMID: 24158538

49. Holmes WR, Mata MA, Edelstein-Keshet L (2015) Local perturbation analysis: A computational tool for biophysical reaction-diffusion models. Biophysical journal 108: 230–236. https://doi.org/10.1016/j.bpj.2014.11.3457 PMID: 25606671

50. Gardner TS, Cantor CR, Collins JJ (2000) Construction of a genetic toggle switch in Escherichia coli. Nature 403: 339–342. https://doi.org/10.1038/35002131 PMID: 10659857

51. Postma M, Bosgraaf L, Loovers HM, Van Haastert PJ (2004) Chemotaxis: signalling modules join hands at front and tail. EMBO reports 5: 35–40. https://doi.org/10.1038/sj.embor.7400051 PMID: 14710184

52. Diz-Muñoz A, Thurley K, Chintamen S, Altschuler SJ, Wu LF, et al. (2016) Membrane tension acts through PLD2 and mTORC2 to limit actin network assembly during neutrophil migration. PLoS Biol 14: e1002474. https://doi.org/10.1371/journal.pbio.1002474 PMID: 27280401

53. Chang YC, Nalbant P, Birkenfeld J, Chang ZF, Bokoch GM (2008) GEF-H1 couples nocodazole-induced microtubule disassembly to cell contractility via RhoA. Molecular biology of the cell 19: 2147–2153. https://doi.org/10.1091/mbc.E07-12-1269 PMID: 18287519

54. Mori Y, Jilkine A, Edelstein-Keshet L (2011) Asymptotic and bifurcation analysis of wave-pinning in a reaction-diffusion model for cell polarization. SIAM J Applied Math 71: 1401–1427. https://doi.org/10.1137/10079118X

55. Weiger MC, Ahmed S, Welf ES, Haugh JM (2010) Directional persistence of cell migration coincides with stability of asymmetric intracellular signaling. Biophysical journal 98: 67–75. https://doi.org/10.1016/j.bpj.2009.09.051 PMID: 20085720

56. Kessler DA, Levine H (2016) Nonlinear self-adapting wave patterns. New Journal of Physics 18: 122001. https://doi.org/10.1088/1367-2630/18/12/122001

57. Bernitt E, Koh CG, Gov N, Döbereiner HG (2015) Dynamics of actin waves on patterned substrates: a quantitative analysis of circular dorsal ruffles. PloS one 10: e0115857. https://doi.org/10.1371/journal.pone.0115857 PMID: 25574668